HHS Public Access

Author manuscript

J Am Chem Soc. Author manuscript; available in PMC 2024 January 11.

Published in final edited form as:

J Am Chem Soc. 2023 January 11; 145(1): 78–88. doi:10.1021/jacs.2c07504.

De Novo Construction of Fluorophores via CO Insertion-initiated Lactamization: A Chemical Strategy Towards Highly Sensitive and Highly Selective Turn-on Fluorescent Probes for Carbon Monoxide

Xiaoxiao Yang[a,‡], **Zhengnan Yuan**[a,‡], **Wen Lu**[a,‡], **Ce Yang**[a], **Minjia Wang**[b], **Ravi Tripathi**[a], **Zach Fultz**[a], **Chalet Tan**[b], **Binghe Wang**[a]

[a] Department of Chemistry and Center for Diagnostics and Therapeutics, Georgia State University, Atlanta, GA 30303 USA

[b] Department of Pharmaceutics and Drug Delivery, University of Mississippi, University, MS 38677 USA

Abstract

Extensive studies in the last few decades have led to the establishment of CO as an endogenous signaling molecule and subsequently exploration of CO's therapeutic roles. At the current state, there is a critical conundrum in CO-related research: the extensive knowledge of CO's biological effects and yet insufficient understanding of the quantitative correlations between CO concentration and biological responses of various natures. This conundrum is partially due to the difficulty in examining precise concentration-response relationships of a gaseous molecule. Another reason is the need for appropriate tools for the sensitive detection and concentration determination of CO in the biological system. We herein report a new chemical approach to the design of fluorescent CO probes through *de novo* construction of fluorophores by a CO insertion-initiated lactamization reaction, which allows for ultra-low background and exclusivity in CO detection. Two series of CO detection probes (CODPs) have been designed and synthesized using this strategy. Using these probes, we have extensively demonstrated their utility in quantifying CO in blood, tissue, and cell culture and in cellular imaging of CO from exogenous and endogenous

Corresponding Authors Xiaoxiao Yang - Department of Chemistry and Center for Diagnostics and Therapeutics, Georgia State University, Atlanta, GA 30303, United States; xyang20@gsu.edu, **Binghe Wang** - Department of Chemistry and Center for Diagnostics and Therapeutics, Georgia State University, Atlanta, GA 30303 United States; wang@gsu.edu.

‡These authors contributed equally.

Author Contributions

The manuscript was written through contributions of all authors. All authors have given approval to the final version of the manuscript.

The authors declare the following competing financial interest(s): X.Y. and B.W. have filed a patent application with Georgia State University (USPTO Application No. 63/395,286) based on this work.

ASSOCIATED CONTENT

SUPPORTING INFORMATION

Supplemental figures, experimental sections, compound characterization, and supplemental video (Video S1) are placed in the Supporting Information for publication. This material is available free of charge at http://pubs.acs.org.

CRYSTALLOGRAPHIC DATA

CCDC 2181545, 2181546, and 2181548 contain the supplementary crystallographic data for this paper (the acronym "COSM" was used for the compounds deposited to CCDC). These data can be obtained free of charge via www.ccdc.cam.ac.uk/data_request/cif, or by emailing data_request@ccdc.cam.ac.uk, or by contacting The Cambridge Crystallographic Data Centre, 12 Union Road, Cambridge CB2 1EZ, UK; fax: +44 1223 336033.

sources. The probes described will enable many biology and chemistry labs to study CO's functions in a concentration-dependent fashion with very high sensitivity and selectivity. The chemical and design principles described will also be applicable in designing fluorescent probes for other small molecules.

Graphical Abstract

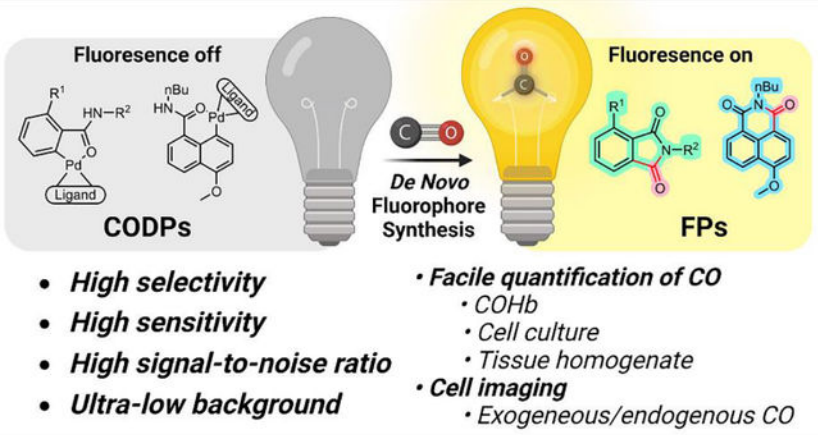

Keywords

Carbon monoxide; fluorescence probe; palladacycle; carbonylation; COHb; tissue CO concentration

Introduction

The paradigm of CO being a notorious toxic gas has been shifted since the first report of the signaling functions of carbon monoxide (CO) in the 1990s. There have been extensive studies of the physiological and pharmacological roles of CO.[1–6] CO is produced endogenously in the human body under normal physiological conditions primely through heme oxygenase-mediated degradation of heme,[2] with a concentration in the blood in the mid micromolar range.[7] CO exerts anti-inflammatory and cyto- and organ-protective effects.[3,8–10] For example, it offers protection in lipopolysaccharide (LPS)-induced inflammation,[11] ischemia-reperfusion injuries,[12,13] chemically[14,15] and rhabdomyolysis[16]-induced organ injuries. The prospect of developing CO into a therapeutic agent for colitis,[17] sickle cell disease,[18] acute kidney injury,[19] among others,[8,20] is supported by the corresponding animal model studies. Extensive efforts have been made in recent years in evaluating inhaled CO gas in clinical trials,[8,21] developing non-gaseous CO delivery approaches,[21] including liquid[18] and foam[20] formulations, metal-based CO-releasing molecules (CORMs),[3,22,23] and organic light-activated CO releasing molecules,[23–27] organic prodrugs[16,28–32] and their formulations.[33] A unique challenge to studying the dose-response relationship of CO is the lack of facile methods for the sensitive and selective determination of its concentration in the blood and various tissues.[34–37] Along this line, there is still much to be desired from existing methods.

There are two mainstream ways of determining CO in biological samples in the literature. The first is direct quantification using gas chromatography (GC) of CO liberated from the tissue using specialized detectors, including a methanizer coupled flame ionization detector (FID),[14] a mercury reduction gas detector (RGD),[38,39] or a semiconductor sensor gas chromatograph (SGC) for needed sensitivity. These delicate gas chromatography instruments are not commonly available in biology labs and require chemistry knowledge in designing experiments and interpreting data, which often pose hurdles to implementing them in CO research. The second approach is to use chemical probes. For example, a cyclodextrin-encapsulated iron(II) porphyrin analog hemoCD1 has been demonstrated to be a powerful chromogenic sensor to determine CO in biological samples by a UV-Vis method.[40,41] Established fluorescent probe approaches include a genetically encoded CO sensing protein (COser)[42] and small molecule reaction-based CO probes (Figure 1A).[43–45] There are two major strategies for designing reaction-based fluorescent probes.[43,46,47] One is to incorporate a transition metal (such as Pd) in a fluorophore, leading to fluorescence quenching.[48] Upon reaction with CO, Pd is removed by either palladium-mediated carbonylation[49] or protonolysis.[50] This “dequenching” strategy has been utilized in designing CO probes such as COP-1[48] and its analogs[44] as well as CC-CO,[51] among others.[43,45] The other strategy is to use an allyl group to cage the fluorophore,[52] which can be removed via the Tsuji-Trost reaction by Pd(0) generated from Pd(II) and CO. These CO probes, especially COP-1,[48] have been extensively used in cellular imaging-based studies and have tremendously aided studies of CO biology. However, depending on the sensing mechanism, the reported probes have their limitations in terms of signal-to-noise ratio (SNR),[42] specificity, and sensitivity towards CO.[53] For dequenching-based probes, presumably due to incomplete quenching of the existing fluorophore by the transition metal, residual background fluorescence is noticeable, leading to a limited SNR. Furthermore, ubiquitous nucleophiles such as thiols in the biological milieu can react and remove the palladium quenching group, which could be seen with the slight turn-on effect by thiol species reported in the literature.[48] For the Tsuji-Trost reaction-based probes, the caging group could potentially be removed by enzymatic catalysis;[54] Pd^{2+} has also been reported to be reduced by ascorbic acid,[55] which may result in false-positive or compatibility issues. It also needs to be noted that there are several nitro-reduction-based probes that initially were reported to detect CO.[43,56,57] However, the detection mechanism was later found to be dependent on the reactivity of the ruthenium-CO complex, not on CO *per se*.[58] Thus, they[43,56,59] should not be regarded as general CO probes, but probes for ruthenium-based CORMs.[42,49,58,60–63] Such results underscore the necessity of using CO gas to authenticate CO sensing and detection.

For improved sensitivity and selectivity to enable CO quantification in biologically relevant samples and to facilitate our undergoing development of CO-based therapies,[16,19,29,34,37] we are interested in developing new chemical strategies for CO fluorescence probes. Our design is based on fluorescence turn-on via *de novo* fluorophore construction for fast, sensitive, and selective (actually exclusive) detection of CO with a high SNR. These probes have been successfully applied in determining CO concentrations in cell culture, blood, and tissue samples in both semi-quantitative and quantitative manners, as well as in fluorescence cellular imaging of CO.

Results and discussion

CO detection chemistry and spectroscopic property profiles of the CO detection probes (CODPs)

We desire fluorescent probes that have a near-zero background for high SNR within a wide range of probe concentrations and exclusively respond to CO. Therefore, instead of using CO-based de-quenching or de-caging chemistry, CO is used as a building block for the *de novo* construction of a fluorophore, leading to exclusivity in sensing and elimination of background fluorescence (Figure 1B). The design takes advantage of a palladium-mediated CO carbonylation reaction followed by a spontaneous lactamization reaction to "construct" the desired fluorophore. Therefore, only upon reacting with CO can fluorescence be turned on. Two fluorogenic scaffolds, phthalimide and naphthalimide fluorophores were chosen to prove the concept (Figure 2).

For the phthalimide scaffold, an O-hydroxyl phthalimide (**FP-1**) with a well-defined excited-state intramolecular proton transfer (ESIPT) fluorescence mechanism[64,65] was chosen as the fluorescent product. The quantum yield (Φ_F) of **FP-1** in pH 7.4 PBS was determined to be 0.23 using quinine sulfate as the reference (Table S2). The first probe series (Figure 2A) was synthesized from 2-amino-6-methoxybenzoic acid (Scheme S1). We did not choose to construct the dimeric palladacycle via ortho-direction as reported for other probes such as COP-1[48] and CC-CO,[51] to avoid high molecular weight and the concern of forming regioisomers.[51] Instead, we introduced an iodo group at the ortho-position of the amide group through diazotization-iodination to direct the oxidative insertion of palladium using tetramethylethyldiamine (TMEDA) as the ligand.[66] Thus, the palladium complex **CODP-101** was synthesized under mild conditions and in good yield. TMEDA was chosen as the ligand due to the stability and aqueous solubility of the resulting complex. Indeed, this molecule reacts with CO and serve as CO fluorescence probe as it is. The iodo group in **CODP-101** was then removed by treating with AgOTf in acetone, forming the palladacycle **CODP-102**. The structure was characterized by NMR and X-ray crystallography (XRC, Figure S20A). Importantly, **CODP-101** and **CODP-102** are soluble and stable in PBS solution at pH 7.4 (Figure S1). Incubating **CODP-102** with CO gas in a headspace vial led to fluorescence turn-on in a linear relationship with CO quantity (Figure 3A,B). The reaction kinetics of **CODP-101** towards CO was found to be the same as **CODP-102** (Figure 3E). Compared to dequenching-based CO probes, the major advantages of this strategy are the high SNR and low background as well as superior selectivity, owning to the completely dark nature of the probe, the large Stokes shift (114 nm) of the product **FP-1**, and the lack of fluorescence interference of the depalladiation species (**DS-1a**) (Figure S5A).

It is well known that similar palladium complexes are reactive toward thiol species.[67] Such reactivity was presumed to cause the response of COP-1 to thiols through protodemetalation,[44] as the depalladation species of the probes may share a similar fluorescence profile with the CO-sensing product. Because thiol species such as H_2S and GSH are present in biological samples, the exclusion of such CO-independent responses can significantly enhance the reliability of CO detection. LC-MS studies showed that upon reacting **CODP-102** with glutathione (GSH) or H_2S (generated from NaHS) in

PBS, the depalladation species (**DS-1a**) was formed (Figure S3A,B). Directly reacting **CODP-102** with two equivalents of NaHS in dimethylacetamide (DMA) gave **DS-1a** as the major product (Figure S3C). However, **DS-1a** did not show any fluorescence at the excitation wavelength used for CO detection, preventing a false-positive response due to depalladiation. The concern of decreasing effective probe concentration by a thiol species can be addressed by increasing the probe concentration without inducing background signal, due to the absence of background fluorescence of the probe and the depalladation species. Since the low background level of **CODP-102** is independent of the probe concentration, it allows for enhancing SNR through increasing probe concentration within a wide concentration range. For example, the SNR of **CODP-102** is 320:1 at 10 μM and 1200:1 at 100 μM (Figure 3C). With respect to selectivity, our design allows for the exclusive detection of CO over other species, demonstrating superior selectivity compared with other palladacycle-based probes. Specifically, **CODP-102** can only be turned on by CO gas as expected (Figure 3D, Figure S2B). No fluorescence change was detected when thiol, persulfide, peroxide, NO^{2-}, among other species, were present.

As for the detection mechanism, we envisioned steps as described in Scheme 1 leading to the “insertion” of CO as one eventual carbonyl group of the phthalimide stucture needed for the fluorescence property of **FP-1**. Specifically, after CO insertion between the palladium and phenyl carbon, a carboxylic acid group is formed upon hydrolysis (Scheme 1). Due to the proximity to the amide nitrogen and the kinetically favorable formation of a five-membered phthalimide ring, the fluorescent *o*-hydroxylphthalimide is formed as the final product. To examine this mechanism, proton NMR, HPLC, and LC-MS were used to study the reaction between **CODP-102** and CO gas. In NMR studies, we monitored the transformation of **CODP-102** in the PBS/D_2O-DMSO solution, which showed the formation of **FP-1** after adding CO gas to the NMR tube (Figure S6). HPLC and LC-MS studies showed that after injecting CO gas into the PBS solution of **CODP-102** and incubating at 37 °C for 30 min, **FP-1** was formed as the major product (Figure S7). Meanwhile, black precipitation (presumably palladium) was observed in the reaction mixture. HPLC analysis also showed a minor peak at 6.2 min in the CO-sensing reaction and in the pure **FP-1** sample. LC-MS studies confirmed it was the ring-open product **IM-1** (Figure S8), an intermediate presented in the hydrolysis equilibrium according to the previous studies.[68] In order to capture the intermediate of the CO detection reaction, an ethanol solution of **CODP-102** was used (Scheme 1). HPLC and LC-MS studies showed the ethyl ester intermediate **IM-2** along with the cyclized product **FP-1** (Figure S7b, S8). After adding PBS to this reaction mixture, **IM-2** was completely converted to **FP-1** almost instantly, indicating the fast intramolecular lactamization reaction in an aqueous solution. Such results also indicate that CO insertion into the palladium complex is likely to be the rate-determining step. In addition, after reacting **CODP-102** with CO gas, the fluorescence intensity was the same as **FP-1** at the same concentration. To this end, the proposed sensing mechanism is consistent with the stoichiometric conversion of the probe to the fluorescent product in PBS solution.

Upon proving the concept with **CODP-101** and **–102**, we sought to optimize the **CODP**s for quantum yield, stability, sensitivity, and response kinetics towards CO for biological

applications. We found that the pKa of the phenol group of **FP-1** rendered the fluorescence pH-sensitive under near-physiological conditions (Figure S2C). To address these issues, the amino analog **FP-4** was selected as a new reporter compound with the quantum yield being substantially increased to 0.33 (Table S2). The maximum excitation/emission wavelength of **FP-4** is blue-shifted by about 10 nm compared to **FP-1** (Figure S5B). Due to the lower pKa of the conjugated acid and improved ESIPT effect of an aniline group, the pH dependency of **FP-4** around physiological pH was largely circumvented (Figure S2D), leading to improved signal stability. Based on **FP-4**, several analogs were designed and synthesized by changing the ligand moiety and the amide chain (Figure 2A). To profile the CO detection reaction kinetics, all **CODP**s were tested at the same concentration with 20-fold molar excess of CO, and the fluorescence intensity was normalized as a percentage of the maximum intensity (Figure 3E). To begin, **CODP-103**, a complex with TMEDA as the ligand, was synthesized (Scheme S2). It showed a faster response to CO when compared to the corresponding hydroxyl analog **CODP-102**. Shortening the amide alkyl substituent from butyl to propyl (**CODP-107**) resulted in a slower response to CO gas. The ligand was then changed to a more electron-withdrawing bipyridyl group. The resulting complex **CODP-105** showed substantially increased reaction kinetics compared to **CODP-107**. Shortening the amide alkyl group from butyl to propyl (**CODP-106**, XRC data: Figure S20B) further increased the reaction kinetics, with the second-order rate constant being 220.6 ± 27.2 $M^{-1}s^{-1}$ (Figure S10). The reaction kinetics of **CODP-106** allowed for almost real-time detection of CO gas (Video S1). **CODP-106** was confirmed to show linear response to CO gas (Figure S9B), high SNR (≈800 at 100 μM, Figure S9C), and excellent selectivity to the point of almost exclusivity (Figure S9D–F), as expected. The quantitative conversion of **CODP-106** to the fluorescent product in a DMA-PBS solution was confirmed by a fluorescence recovery assay (Figure S11). Interestingly, we applied the same bipyridyl ligand to modify **CODP-102**. The resulting palladacycle **CODP-104** showed a much slower response to CO than **CODP-102**. The second-order reaction rate constant was determined to be 13.8 ± 1.4 $M^{-1}s^{-1}$. The CO-sensing kinetic parameters generally fall within limits defined by **CODP-104** and **CODP-106** (Figure 3E). The results indicate the intricate effects of the substitution of the phenyl ring and the palladium ligand on the CO insertion reaction.

The sensitivity of **CODP-102**, **CODP-103**, and **CODP-106** was studied by incubating them with 1.6~8 ppm CO in the air in a headspace vial (see SI for details). Due to their high SNR, we anticipated the feasibility of using these probes at high concentrations for increased sensitivity. To test this assumption, sensitivity was tested at both low (100 μM) and high (1 mM) concentrations. The theoretical detection limit was determined to be about 0.1–0.2 ppm for **CODP-102**, **103**, and **106** dissolved in DMA (Table S1–1), which is the equivalent of 0.45–0.9 nM in solution according to Henry's law.[69] As expected, a higher probe concentration gave a higher sensitivity, as shown by the lower detection limit in general (Table S1–1). The high sensitivity coupled with the high SNR allows for robust determination of CO concentrations in the biospecimen discussed in later application sections. In comparison, the detection limit using GC with 100 μL gas injection is 0.5 ppm for methanizer FID, according to the manufacturers' specifications. Therefore, these fluorescence probes are at the sensitivity level of the methanizer-FID-GC, which is sufficient for detecting basal CO levels *in vivo*.

When we applied **CODP-102** and **CODP-106** in cellular imaging studies, we found poor accumulation and undesirable photostability of the fluorescent products **FP-1** and **FP-4** in the cell. We sought to tackle this issue by applying our CO sensing strategy to construct probes based on the 1,8-naphthalimide fluorophore, which is known for good photostability, cell permeability,[70] and tunable quantum yield.[71] As a result, two naphthalic amide-based CO probes **CODP-201** and **CODP-202** were designed and synthesized (Scheme S3) by using a similar chemical strategy (Figure 2B). Bipyridine and TMEDA were studied as ligands. The attempt to synthesize the complex with TMEDA ligand failed due to spontaneous decomposition during the reaction. On the other hand, the bipyridyl ligand palladium complex **CODP-201** was stable during synthesis. The bromide in **CODP-201** was removed by AgOTf to form the six-membered palladacycle **CODP-202**. Both structures were confirmed by XRC (Figure S20C,D). **CODP-201** and **–202** were found to be stable for at least 1 h in PBS solution at 37 °C (Figure S12). The apparent reaction kinetics of **CODP-202** towards CO was determined to be as fast as **CODP-106** (Figure S13C). The formation of a six-membered naphthalimide fluorescent product **FP-5** by reacting **CODP-202** with CO in PBS solution was confirmed by LCMS studies (Figure S14). The quantum yield of **FP-5** was determined to be 0.82 in water (Table S2). Importantly, the depalladiation specie **DP-2** also features an excitation spectrum distinctively different from that of the CO-sensing product **FP-5** (Figure S5C), which allows for high SNR (Figure 4) and similar exclusivity in analyte detection (Figure S13). The CO detection limits of **CODP-201** and **CODP-202** were determined to be 2.74 nM and 2.06 nM (Table S1–2), respectively, by using 20 μM of the probe and assuming CO solubility was 1 mM in PBS at 760 mmHg CO partial pressure.[72] It is reported that the endogenous CO concentration in the mammalian cell is in the micromolar range.[40] Therefore, **CODP-202** should be capable of detecting CO generated endogenously in the cell culture.

Application of CODPs.

CODP-102, –103, –106, and **–202** were chosen to demonstrate their utility in two key CO determination applications for biological research, 1) measuring CO contents in cell culture, blood, and tissue samples (Figure 5); and 2) imaging intracellular CO accumulation. Each **CODP** has its own physical, chemical, and biological characteristics suited for different applications.

Relative quantification of CO in blood and cell culture.

With the TMEDA ligand and triflate salt, **CODP-102** and **–103** showed higher water solubility (*c.a.* 5 mM) compared to **CODP-106** (*c.a.* 100 μM) and **CODP-202** (*c.a.* 50 μM). The fluorescent products of **CODP-102** and **–103** are stable in serum. Although **FP-1** showed pH-dependent fluorescence, the blood pH is not expected to fluctuate significantly. Buffering the testing fluid with PBS at 10 mM (1×) was sufficient to stabilize the pH in our studies. Therefore, both **CODP-102** and **–103** were selected to measure mouse blood COHb. As the mouse blood hemoglobin tetramer concentration is about 2 mM,[73] 100% COHb should give a CO concentration of about 8 mM. To directly test COHb levels up to 50%, the probe concentration should be at least 4 mM. Even at this high concentration, the background signal of our probes was negligible. By directly incubating **CODP-102** at

a concentration of 10 mM with blood samples of various COHb levels pre-determined by a CO-oximeter, an excellent correlation between the fluorescence intensity and the COHb level was established (Figure 6A,B). By using this standard curve, the COHb level of an unknown partially CO-saturated blood sample with a fluorescence intensity of 117.48 a.u. was calculated to be 7.9%. CO-oximeter reading of the same sample showed a COHb level of 8.2 ± 0.45%, demonstrating excellent consistency.

To determine COHb levels without a CO-oximeter, a definitive COHb calibration level of the blood is needed. It has been reported that pre-saturation of blood with pure CO gas leads to about a 90% COHb level.[74] In our hands, the 90% COHb level was also verified to be consistent among the CO-saturated blood collected from five mice (Figure S15).

By assigning the COHb level of CO saturated-N_2 flushed blood to be 90% and serially diluting by normal blood, a calibration curve can be established with **CODP**s. Thus, the COHb level of an unknown sample can be determined by the probe with a fluorescence microplate reader without using a CO-oximeter, GC, or even fluorospectrometer (Figure S16). Since most research labs do not readily have access to a CO-oximeter, there is a great need for alternative COHb determination approaches. The method described herein can address this unmet need in CO research. The protocol we have developed based on **CODP**s was successfully verified in two *ex-vivo* experiments. After orally administering the CO prodrug **CO-306**[16] and its activated charcoal formulation **AC-306**[33] in mice, blood COHb levels determined by **CODP-102** and **–103** were in excellent agreement with the ones determined with a CO-oximeter (Figure 6C, 6D). The same methodology can also be applied in cellular experiments to determine changes in CO levels induced by external CO sources such as CO gas or increased endogenous CO production via induction of HO-1 expression. Specifically, HeLa cells were incubated with 250 ppm CO gas for 2 h or with 0.3 μM CDDO-Me for 6 h followed by collection with a cell scraper. HO-1 inducer CDDO-Me[75] was used due to the lack of spectroscopic interference in the fluorescence experiments compared to the commonly used chromogenic hemin.[40] Incubation of the washed cell pellets with 100 μM **CODP-103** followed by fluorescence measurements with a microplate reader showed that the fluorescence signal increased by about 28% after CO gas treatment and by 7.5% after CDDO-Me treatment when compared with the 0.5% DMSO vehicle treatment controls (Figure 6E). Western blot confirmed that CDDO-Me treatment significantly increased HO-1 expressions in HeLa cells (Figure 6F), which presumably accounted for the elevated CO production.

Determination of absolute amounts of CO in tissue and cell culture samples.

In understanding CO exposure levels in the context of pharmacokinetic considerations, the bioavailability of the delivered CO is commonly evaluated by calculating the area under the curve (AUC) of COHb levels.[37] Tissue CO concentration, on the other hand, has not been well defined in most CO delivery studies, presumably due to limited access to appropriate detection methods. The endogenous CO concentrations in various organs have been determined to be about 2–10 pmol/mg in mouse tissues using an RGD-GC method.[35] Theoretically, if about 100 mg of tissue releases all bound CO to 1 ml headspace in a headspace vial, it should give at least 4.5 ppm CO. We sought to test if **CODP-106** with a

detection limit of 0.1 ppm and fast reaction kinetics could be used to determine the tissue CO concentration quantitatively.

To develop the quantification method, **CODP-106** was dissolved in 50 μL degassed DMA at a concentration of 1 mM and sealed in a 0.5-ml vacuumed headspace vial with PTFE/silicone crimp septum. This probe-charged headspace vial (CO detection vial) was used as a CO "detector" by injecting CO-containing gas followed by incubation and measurement of fluorescence intensity with either a fluorometer or a plate reader (Figure S16). Quantification was achieved via an external standard curve method by injecting 250 μL of standard CO calibration gas (10–100 ppm CO in the air) into the detection vial. The excellent reproducibility and goodness-of-fit indicate the soundness of the experimental setup (Figure 7A). To verify its utility in an *ex-vivo* study of CO donor administration, we harvested the perfused organ tissues from the same mice dosed with 200 mg/kg **CO-306**, which were used for the aforementioned COHb analysis. Aliquots of liver and kidney homogenates were concomitantly tested with **CODP-106** and a methanizer-FID-GC (see SI for detailed methods). Protein-bound CO was liberated in the headspace vial by 3% 5-sulfosalicylic acid (SSA) according to an established procedure.[35, 38] Liver tissue CO concentration was determined to be about 5 pmol/mg for the control and 31 pmol/mg for the **CO-306**-treated group. Kidney tissue CO concentration was determined to be 11 pmol/mg for the control and 26 pmol/mg for the **CO-306**-treated group. There was no statistical difference between the results determined by GC and the CO probe (Figure 7B, 7C), confirming that our CO detection protocol using **CODP-106** was able to quantify CO in tissue samples with accuracy and reproducibility on par with that of a methanizer-FID-GC system, which is regarded as the "gold standard" for determining tissue CO concentrations. The tissue CO concentration of the control mice was also in a similar range as tested with an RGD-GC method by Vreman *et al.*,[35] further supporting the reproducibility of our methods.

Similarly, **CODP-106** CO detection tube can also be used to determine CO concentrations in cell culture. After treating HeLa cells with 250 ppm CO gas or **CO-111** (50 μM),[14] a CO prodrug, for 2 h, CO concentration increased substantially from 25 pmol/10^6 cells to 92 pmol/10^6 cells, and 203 pmol/10^6 cells, respectively (Figure 7D). Since cells were washed with PBS twice before denaturing and CO determination, the substantially higher CO concentration in the CO-111 treatment group could be partially attributed to the combined CO amounts from hemoprotein-bound CO and the residual intracellular CO prodrug. However, the residual amount is expected to be small because of the short half-life of this prodrug (15–25 min).[14, 77] Thus, for a quick comparison, 50 μM of prodrug **CO-111** was able to deliver more CO in cell culture than 250 ppm of CO gas during a 2-h period. To this end, we have demonstrated that **CODP-102**, **–103**, and **–106** can be used to determine CO concentrations in cell culture, blood, and tissue in a semi-quantitative and quantitative manner with excellent reproducibility and accuracy.

Fluorescence imaging of CO in cell culture.

As a key visualization method in chemical biology research, fluorescence imaging has significantly aided the understanding of CO's function and the development of various useful CO donors capable of delivering CO to the intracellular space.[77] The fluorescence

product of the **CODP-10X** series showed rapid diffusion and low photostability. On the other hand, the **CODP-20X** series have similar advantageous features of high selectivity, high sensitivity, and low background, and yet the fluorescence product (**FP-5**) has higher photostability and quantum yield. Thus, **CODP-201** and **–202** were used to demonstrate their feasibility in cellular image applications. They showed no cytotoxicity to HeLa cells at concentrations lower than 50 μM within 24 h (Figure S18). As a trifluoromethanesulfonic salt, **CODP-202** has a higher aqueous solubility than **CODP-201**. Both can be used in cell imaging CO from various sources, including CO gas, a CO prodrug (CO-201),[78] and CORM-401,[79] which were chosen partially because of the lack of fluorescence interference. As shown in Figure 8 and Figure S19, live HeLa cells showed strong blue fluorescence under the blue DAPI channel (385/455 nm) after treatment with CO followed by the addition of 20 μM **CODP-201** and **–202**. In contrast, the control group without CO treatment did not show any fluorescence under the same imaging conditions. The low background fluorescence in the vehicle control group again demonstrates the advantage of the fluorescence turn-on strategy based on *de novo* construction. Further, **CODP-202** was also able to sense the increase in endogenous CO production induced by 0.3 μM CDDO-Me. However, a longer exposure time (6 s) was needed to image CO produced endogenously.

Conclusion

The fledgling CO research field is at a critical juncture in need of careful studies to understand dose-response relationships. There is an unmet need for tools that allow for highly sensitive and selective detection of CO in a variety of samples. In this study, we developed a *de novo* fluorophore construction approach to the design of CO probes with three key advantageous features: (1) the probe is completely dark, allowing for superior sensitivity, SNR, and a wide linearity range for CO determination; (2) depalladation by thiols leads to no fluorescence response at the expected excitation wavelength, preventing false-positive response; and (3) only CO insertion allows for the construction of a fluorophore, allowing for the exclusive detection of CO. Such features allowed us to apply **CODP-102**, **–103**, and **–106** in quantifying CO in cell culture, blood, and tissue samples for the first time, to the best of our knowledge. The experimental protocols we developed along the way are robust and can be easily adopted by common biology labs without special chemistry equipment or expertise. The same design strategy has been applied to naphthylamide-based fluorophores, which have shown to be very useful for detecting and imaging exogenous CO from CO gas or CO donors in live cells. **CODP-202** is also able to detect endogenous CO production upon stimulation by an HO-1 inducer CDDO-Me. Overall, we have shown the advantages of the new *de-novo* fluorophore construction strategy in developing fluorescence probes for CO. We hope the work described will not only facilitate research in understanding CO's biological functions and therapeutic potential but also inspire new designs of fluorescent probes for other molecules in the future.

Supplementary Material

Refer to Web version on PubMed Central for supplementary material.

ACKNOWLEDGMENT

The authors thank Dr. John Bacsa at Emory University for determining the crystal structures of the palladium complexes. Mass spectrometry analyses were conducted by the Georgia State University Mass Spectrometry Facilities, which are partially supported by an NIH grant for the purchase of a Waters Xevo G2-XS Mass Spectrometer (1S10OD026764–01).

Funding Sources

The authors gratefully acknowledge partial financial support from the National Institutes of Health (R01DK119202 for work on CO and colitis; R01DK128823 for work on CO and acute kidney injury), the Georgia Research Alliance for an Eminent Scholar fund (B.W.), and internal resources at Georgia State University. Z.Y. acknowledges the financial support of the GSU Brains and Behaviors program through an internal fellowship, and Z.F. acknowledges the financial support of the Center for Diagnostics and Therapeutics through a CDT Fellowship.

REFERENCES

(1). Verma A; Hirsch DJ; Glatt CE; Ronnett GV; Snyder SH, Carbon monoxide: a putative neural messenger. Science. 1993, 259, 381–384. [PubMed: 7678352]

(2). Wu L; Wang R, Carbon monoxide: endogenous production, physiological functions, and pharmacological applications. Pharmacol. Rev. 2005, 57, 585–630. [PubMed: 16382109]

(3). Motterlini R; Otterbein LE, The therapeutic potential of carbon monoxide. Nat. Rev. Drug. Discov. 2010, 9, 728–743. [PubMed: 20811383]

(4). Heinemann SH; Hoshi T; Westerhausen M; Schiller A, Carbon monoxide-physiology, detection and controlled release. ChemComm. 2014, 50, 3644–3660.

(5). Hopper PC; Meinel L; Steiger C; Otterbein EL, Where is the clinical breakthrough of heme oxygenase-1/carbon monoxide therapeutics? Curr. Pharm. Des 2018, 24, 2264–2282. [PubMed: 30039755]

(6). Wang B; Otterbein LE Carbon Monoxide in Drug Discovery: Basics, Pharmacology, and Therapeutic Potential. John Wiley and Sons: Hoboken, New Jersey, 2022.

(7). Coburn RF; Forster RE; Kane PB, Considerations of the physiological variables that determine the blood carboxyhemoglobin concentration in man. J. Clin. Invest. 1965, 44, 1899–1910. [PubMed: 5845666]

(8). Chu LM; Shaefi S; Byrne JD; Alves de Souza RW; Otterbein LE, Carbon monoxide and a change of heart. Redox Biol. 2021, 48, 102183. [PubMed: 34764047]

(9). Ryter SW; Alam J; Choi AM, Heme oxygenase-1/carbon monoxide: from basic science to therapeutic applications. Physiol. Rev. 2006, 86, 583–650. [PubMed: 16601269]

(10). Yang X; Lu W; Hopper CP; Ke B; Wang B, Nature’s marvels endowed in gaseous molecules I: Carbon monoxide and its physiological and therapeutic roles. Acta. Pharm. Sin. B. 2021, 11, 1434–1445. [PubMed: 34221861]

(11). Otterbein LE; Bach FH; Alam J; Soares M; Tao Lu H; Wysk M; Davis RJ; Flavell RA; Choi AM, Carbon monoxide has anti-inflammatory effects involving the mitogen-activated protein kinase pathway. Nat. Med. 2000, 6, 422–428. [PubMed: 10742149]

(12). Correa-Costa M; Gallo D; Csizmadia E; Gomperts E; Lieberum J-L; Hauser CJ; Ji X; Wang B; Câmara NOS; Robson SC; Otterbein LE, Carbon monoxide protects the kidney through the central circadian clock and CD39. Proc. Natl. Acad. Sci. U.S.A. 2018, 115, E2302–E2310. [PubMed: 29463714]

(13). Kaizu T; Ikeda A; Nakao A; Tsung A; Toyokawa H; Ueki S; Geller DA; Murase N, Protection of transplant-induced hepatic ischemia/reperfusion injury with carbon monoxide via MEK/ERK1/2 pathway downregulation. Am. J. Physiol. Gastrointest. Liver Physiol 2008, 294, G236–G244. [PubMed: 18006605]

(14). Bakalarz D; Surmiak M; Yang X; Wójcik D; Korbut E; Śliwowski Z; Ginter G; Buszewicz G; Brzozowski T; Cieszkowski J; Głowacka U; Magierowska K; Pan Z; Wang B; Magierowski M, Organic carbon monoxide prodrug, BW-CO-111, in protection against chemically induced gastric mucosal damage. Acta. Pharm. Sin. B. 2020, 11, 456–475. [PubMed: 33643824]

(15). Bakhautdin B; Das D; Mandal P; Roychowdhury S; Danner J; Bush K; Pollard K; Kaspar JW; Li W; Salomon RG; McMullen MR; Nagy LE, Protective role of HO-1 and carbon monoxide in ethanol-induced hepatocyte cell death and liver injury in mice. J. Hepatol. 2014, 61, 1029–37. [PubMed: 24946281]

(16). De La Cruz LK; Yang X; Menshikh A; Brewer M; Lu W; Wang M; Wang S; Ji X; Cachuela A; Yang H; Gallo D; Tan C; Otterbein L; de Caestecker M; Wang B, Adapting decarbonylation chemistry for the development of prodrugs capable of in vivo delivery of carbon monoxide utilizing sweeteners as carrier molecules. Chem. Sci. 2021, 12, 10649–10654. [PubMed: 34447558]

(17). Steiger C; Uchiyama K; Takagi T; Mizushima K; Higashimura Y; Gutmann M; Hermann C; Botov S; Schmalz HG; Naito Y; Meinel L, Prevention of colitis by controlled oral drug delivery of carbon monoxide. J. Control. Release. 2016, 239, 128–36. [PubMed: 27578097]

(18). Belcher JD; Gomperts E; Nguyen J; Chen C; Abdulla F; Kiser ZM; Gallo D; Levy H; Otterbein LE; Vercellotti GM, Oral carbon monoxide therapy in murine sickle cell disease: Beneficial effects on vaso-occlusion, inflammation and anemia. PLoS One 2018, 13, e0205194. [PubMed: 30308028]

(19). Yang X; de Caestecker M; Otterbein LE; Wang B Carbon monoxide: An emerging therapy for acute kidney injury. Med. Res. Rev. 2020, 40, 1147–1177. [PubMed: 31820474]

(20). Byrne JD; Gallo D; Boyce H; Becker SL; Kezar KM; Cotoia AT; Feig VR; Lopes A; Csizmadia E; Longhi MS; Lee JS; Kim H; Wentworth AJ; Shankar S; Lee GR; Bi J; Witt E; Ishida K; Hayward A; Kuosmanen JLP; Jenkins J; Wainer J; Aragon A; Wong K; Steiger C; Jeck WR; Bosch DE; Coleman MC; Spitz DR; Tift M; Langer R; Otterbein LE; Traverso G, Delivery of therapeutic carbon monoxide by gas-entrapping materials. Sci. Transl. Med. 2022, 14, eabl4135. [PubMed: 35767653]

(21). Yang X; Ke B; Lu W; Wang B CO as a therapeutic agent: Discovery and delivery forms. Chin. J. Nat. Med. 2020, 18, 284–295. [PubMed: 32402406]

(22). Mann BE, CO-releasing molecules: a personal view. Organometallics 2012, 31, 5728–5735.

(23). Lazarus LS; Benninghoff AD; Berreau LM, Development of triggerable, trackable, and targetable carbon monoxide releasing molecules. Acc. Chem. Res. 2020, 53 (10), 2273–2285. [PubMed: 32929957]

(24). Peng P; Wang C; Shi Z; Johns VK; Ma L; Oyer J; Copik A; Igarashi R; Liao Y, Visible-light activatable organic CO-releasing molecules (PhotoCORMs) that simultaneously generate fluorophores. Org. Biomol. Chem. 2013, 11, 6671–6674. [PubMed: 23943038]

(25). Poloukhtine A; Popik VV, Mechanism of the cyclopropenone decarbonylation reaction. A density functional theory and transient spectroscopy study. J. Phys. Chem. A 2006, 110, 1749–1757. [PubMed: 16451004]

(26). Štacková L; Russo M; Muchová L; Orel V; Vítek L; Štacko P; Klán P, Cyanine-flavonol hybrids for near-infrared light-activated delivery of carbon monoxide. Eur. J. Chem. 2020, 26, 13184–13190.

(27). Russo M; Orel V; Štacko P; Šranková M; Muchová L; Vítek L; Klán P, Structure–photoreactivity relationship of 3-Hydroxyflavone-based CO-releasing Molecules. J. Org. Chem. 2022, 87, 4750–4763. [PubMed: 35282677]

(28). Kueh JTB; Stanley NJ; Hewitt RJ; Woods LM; Larsen L; Harrison JC; Rennison D; Brimble MA; Sammut IA; Larsen DS, Norborn-2-en-7-ones as physiologically-triggered carbon monoxide-releasing prodrugs. Chem. Sci. 2017, 8 (8), 5454–5459. [PubMed: 28970925]

(29). Ji X; Wang B, Strategies toward organic carbon monoxide prodrugs. Acc. Chem. Res. 2018, 51, 1377–1385. [PubMed: 29762011]

(30). Thiang Brian Kueh J; Seifert-Simpson JM; Thwaite SH; Rodgers GD; Harrison JC; Sammut IA; Larsen DS, Studies towards non-toxic, water soluble, vasoactive norbornene organic carbon monoxide releasing molecules. Asian J. Org. Chem. 2020, 9, 2127–2135.

(31). Min Q; Ni Z; You M; Liu M; Zhou Z; Ke H; Ji X, Chemiexcitation-triggered prodrug activation for targeted carbon monoxide delivery. Angew. Chem. Int. Ed. Engl. 2022, 61, e202200974. [PubMed: 35385195]

(32). Xing L; Wang B; Li J; Guo X; Lu X; Chen X; Sun H; Sun Z; Luo X; Qi S; Qian X; Yang Y, A fluorogenic ONOO–-triggered carbon monoxide donor for mitigating brain ischemic damage. J. Am. Chem. Soc. 2022, 144, 2114–2119. [PubMed: 35080381]

(33). Yang X; Lu W; Wang M; De La Cruz LK; Tan C; Wang B, Activated charcoal dispersion of carbon monoxide prodrugs for oral delivery of CO in a pill. Int. J. Pharm. 2022, 618, 121650. [PubMed: 35276229]

(34). Yang X; Lu W; Wang M; Tan C; Wang B, "CO in a pill": Towards oral delivery of carbon monoxide for therapeutic applications. J. Control. Release. 2021, 338, 593–609. [PubMed: 34481027]

(35). Vreman HJ; Wong RJ; Kadotani T; Stevenson DK, Determination of carbon monoxide (CO) in rodent tissue: effect of heme administration and environmental CO exposure. Anal. Biochem. 2005, 341, 280–289. [PubMed: 15907874]

(36). Vreman HJ; Stevenson DK; Henton D; Rosenthal P, Correlation of carbon monoxide and bilirubin production by tissue homogenates. J. Chromatogr. 1988, 427, 315–319. [PubMed: 3410913]

(37). Wang M; Yang X; Pan Z; Wang Y; De La Cruz LK; Wang B; Tan C, Towards "CO in a pill": Pharmacokinetic studies of carbon monoxide prodrugs in mice. J. Control. Release. 2020, 327, 174–185. [PubMed: 32745568]

(38). Vreman HJ; Wong RJ; Stevenson DK; Smialek JE; Fowler DR; Li L; Vigorito RD; Zielke HR, Concentration of carbon monoxide (CO) in postmortem human tissues: effect of environmental CO exposure. J. Forensic. Sci. 2006, 51, 1182–1190. [PubMed: 17018107]

(39). Cronje FJ; Carraway MS; Freiberger JJ; Suliman HB; Piantadosi CA, Carbon monoxide actuates O(2)-limited heme degradation in the rat brain. Free Radic. Biol. Med. 2004, 37, 1802–1812. [PubMed: 15528039]

(40). Minegishi S; Yumura A; Miyoshi H; Negi S; Taketani S; Motterlini R; Foresti R; Kano K; Kitagishi H, Detection and removal of endogenous carbon monoxide by selective and cell-permeable hemoprotein model complexes. J. Am. Chem. Soc. 2017, 139, 5984–5991. [PubMed: 28388069]

(41). Mao Q; Kawaguchi AT; Mizobata S; Motterlini R; Foresti R; Kitagishi H, Sensitive quantification of carbon monoxide in vivo reveals a protective role of circulating hemoglobin in CO intoxication. Commun. Biol 2021, 4, 425. [PubMed: 33782534]

(42). Yuan L; Lin W; Tan L; Zheng K; Huang W, Lighting up carbon monoxide: fluorescent probes for monitoring CO in living cells. Angew. Chem. Int. Ed. Engl. 2013, 52, 1628–1630. [PubMed: 23239366]

(43). Mukhopadhyay S; Sarkar A; Chattopadhyay P; Dhara K, Recent advances in fluorescence light-up endogenous and exogenous carbon monoxide detection in biology. Chem. Asian. J. 2020, 15, 3162–3179. [PubMed: 33439547]

(44). Morstein J; Höfler D; Ueno K; Jurss JW; Walvoord RR; Bruemmer KJ; Rezgui SP; Brewer TF; Saitoe M; Michel BW; Chang CJ, Ligand-directed approach to activity-based sensing: developing palladacycle fluorescent probes that enable endogenous carbon monoxide detection. J. Am. Chem. Soc. 2020, 142, 15917–15930. [PubMed: 32872768]

(45). Walvoord RR; Schneider MR; Michel BW Fluorescent probes for intracellular carbon monoxide detection. In Carbon Monoxide in Drug Discovery: Basics, Pharmacology, and Therapeutic Potential. John Wiley and Sons: Hoboken, New Jersy, 2022; pp 321–343.

(46). Heinemann SH; Hoshi T; Westerhausen M; Schiller A, Carbon monoxide-physiology, detection and controlled release. ChemComm. 2014, 50, 3644–3660.

(47). Yan L; Yang H; Zhang S; Zhou C; Lei C, A critical review on organic small fluorescent probes for monitoring carbon monoxide in biology. Crit. Rev. Anal. Chem. 2022, 1–15.

(48). Michel BW; Lippert AR; Chang CJ, A reaction-based fluorescent probe for selective imaging of carbon monoxide in living cells using a palladium-mediated carbonylation. J. Am. Chem. Soc. 2012, 134, 15668–15671. [PubMed: 22970765]

(49). Nieto S; Arnau P; Serrano E; Navarro R; Soler T; Cativiela C; Urriolabeitia EP, Functionalization of methyl (R)-phenylglycinate through orthopalladation: C–Hal, C–O, C–N, and C–C bond coupling. Inorg. Chem. 2009, 48, 11963–11975. [PubMed: 19911828]

(50). García-López J-A; Oliva-Madrid M-J; Saura-Llamas I; Bautista D; Vicente J, Reactivity toward CO of eight-membered palladacycles derived from the insertion of alkenes into the Pd–C bond of cyclopalladated primary arylalkylamines of pharmaceutical Interest. Synthesis of tetrahydrobenzazocinones, ortho-functionalized phenethylamines, ureas, and an isocyanate. Organometallics. 2012, 31, 6351–6364.

(51). Zheng K; Lin W; Tan L; Chen H; Cui H, A unique carbazole–coumarin fused two-photon platform: development of a robust two-photon fluorescent probe for imaging carbon monoxide in living tissues. Chem. Sci. 2014, 5, 3439–3448.

(52). Feng W; Liu D; Feng S; Feng G, Readily available fluorescent probe for carbon monoxide imaging in living cells. Anal. Chem. 2016, 88, 10648–10653. [PubMed: 27728973]

(53). Tang Y; Ma Y; Yin J; Lin W, Strategies for designing organic fluorescent probes for biological imaging of reactive carbonyl species. Chem. Soc. Rev. 2019, 48, 4036–4048. [PubMed: 31187789]

(54). Huang TL; Szekacs A; Uematsu T; Kuwano E; Parkinson A; Hammock BD, Hydrolysis of carbonates, thiocarbonates, carbamates, and carboxylic esters of alpha-naphthol, beta-naphthol, and p-nitrophenol by human, rat, and mouse liver carboxylesterases. Pharm. Res. 1993, 10, 639–648. [PubMed: 8321828]

(55). Castegnaro MV; Kilian AS; Baibich IM; Alves MCM; Morais J, On the reactivity of carbon supported Pd nanoparticles during NO reduction: Unraveling a metal–support redox interaction. Langmuir. 2013, 29, 7125–7133. [PubMed: 23683147]

(56). Das B; Lohar S; Patra A; Ahmmed E; Mandal SK; Bhakta JN; Dhara K; Chattopadhyay P, A naphthalimide-based fluorescence ‘‘turn-on’’ chemosensor for highly selective detection of carbon monoxide: Imaging applications in living cells. New J. Chem. 2018, 42, 13497–13502.

(57). Tang Z; Song B; Ma H; Luo T; Guo L; Yuan J, Mitochondria-targetable ratiometric time-gated luminescence probe for carbon monoxide based on lanthanide complexes. Anal. Chem. 2019, 91, 2939–2946. [PubMed: 30674191]

(58). Yuan Z; Yang X; De La Cruz LK; Wang B, Nitro reduction-based fluorescent probes for carbon monoxide require reactivity involving a ruthenium carbonyl moiety. ChemComm. 2020, 56, 2190–2193.

(59). Yue L; Tang Y; Huang H; Song W; Lin W, A fluorogenic probe for detecting CO with the potential integration of diagnosis and therapy (IDT) for cancer. Sens. Actuators B: Chem. 2021, 344, 130245.

(60). Zhou E; Gong S; Xia Q; Feng G, In vivo imaging and tracking carbon monoxide-releasing molecule-3 with an NIR fluorescent probe. ACS Sensors. 2021, 6, 1312–1320. [PubMed: 33576235]

(61). Feng W; Feng S; Feng G, A fluorescent ESIPT probe for imaging CO-releasing molecule-3 in living systems. Anal. Chem. 2019, 91, 8602–8606. [PubMed: 31179693]

(62). Xu H; Zong S; Xu H; Tang X; Li Z, Detection and imaging of carbon monoxide releasing molecule-2 in HeLa cells and zebrafish using a metal-Free near-infrared fluorescent off–on probe. Spectrochim. Acta. A Mol. Biomol. Spectrosc. 2022, 272, 120964. [PubMed: 35151164]

(63). Li S; Yang K; Zeng J; Xia Y; Cheng D; He L, A NIR-emissive probe with a remarkable Stokes shift for CO-releasing molecule-3 detection in cells and in vivo. Analyst. 2022, 147 (6), 1169–1174. [PubMed: 35188519]

(64). Sedgwick AC; Wu L; Han HH; Bull SD; He XP; James TD; Sessler JL; Tang BZ; Tian H; Yoon J, Excited-state intramolecular proton-transfer (ESIPT) based fluorescence sensors and imaging agents. Chem. Soc. Rev. 2018, 47, 8842–8880. [PubMed: 30361725]

(65). Tang J; Wu H; Yin S; Han Y, An ESIPT-based fluorescent probe for Hg2+ in aqueous solution and its application in live-cell imaging. Tetrahedron Lett. 2019, 60, 541–546.

(66). Frutos-Pedreño R; González-Herrero P; Vicente J; Jones PG, Reactivity of ortho-palladated benzamides toward CO, isocyanides, and alkynes. Synthesis of functionalized isoindolin-1-ones and 4,5-disubstituted benzo[c]azepine-1,3-diones. Organometallics. 2013, 32, 4664–4676.

(67). Li J; Yang S; Wu W; Jiang H, Recent developments in palladium-catalyzed C–S bond formation. Org. Chem. Front. 2020, 7, 1395–1417.

(68). Cheong MY; Ariffin A; Khan MN, Kinetic coupled with UV spectral evidence for near-irreversible nonionic micellar binding of N-benzylphthalimide under the typical reaction conditions: an observation against a major assumption of the pseudophase micellar model. J. Phys. Chem. B 2007, 111, 12185–12194. [PubMed: 17914797]

(69). Baruah S; Dutta NN; Patil GS, Solubility of carbon monoxide in 1,1,1-trichloroethane, *N,N*-dimethylacetamide, dibutyl phthalate, and their mixtures. J. Chem. Eng. Data. 1992, 37, 291–293.

(70). Choi S-A; Park CS; Kwon OS; Giong H-K; Lee J-S; Ha TH; Lee C-S, Structural effects of naphthalimide-based fluorescent sensor for hydrogen sulfide and imaging in live zebrafish. Sci. Rep. 2016, 6 (1), 26203. [PubMed: 27188400]

(71). Liu X; Qiao Q; Tian W; Liu W; Chen J; Lang MJ; Xu Z, Aziridinyl fluorophores demonstrate bright fluorescence and superior photostability by effectively inhibiting twisted intramolecular charge transfer. J. Am. Chem. Soc. 2016, 138, 6960–6963. [PubMed: 27203847]

(72). Almeida AS; Queiroga CS; Sousa MF; Alves PM; Vieira HL, Carbon monoxide modulates apoptosis by reinforcing oxidative metabolism in astrocytes: Role of Bcl-2. J. Biol. Chem. 2012, 287, 10761–10770. [PubMed: 22334654]

(73). Raabe BM; Artwohl JE; Purcell JE; Lovaglio J; Fortman JD, Effects of weekly blood collection in C57BL/6 mice. J. Am. Assoc. Lab. Anim. Sci. 2011, 50, 680–685. [PubMed: 22330715]

(74). Bickler MP; Rhodes LJ, Accuracy of detection of carboxyhemoglobin and methemoglobin in human and bovine blood with an inexpensive, pocket-size infrared scanner. PLoS One. 2018, 13, e0193891. [PubMed: 29513738]

(75). Wang YY; Yang YX; Zhe H; He ZX; Zhou SF, Bardoxolone methyl (CDDO-Me) as a therapeutic agent: an update on its pharmacokinetic and pharmacodynamic properties. Drug Des. Devel. Ther. 2014, 8, 2075–2088.

(76). Pan Z; Chittavong V; Li W; Zhang J; Ji K; Zhu M; Ji X; Wang B, Organic CO prodrugs: structure-CO-release rate relationship studies. Chem. Eur. J. 2017, 23, 9838–9845. [PubMed: 28544290]

(77). Ohata J; Bruemmer KJ; Chang CJ, Activity-based sensing methods for monitoring the reactive carbon species carbon monoxide and formaldehyde in living systems. Acc. Chem. Res. 2019, 52, 2841–2848. [PubMed: 31487154]

(78). Ji X; De La Cruz LKC; Pan Z; Chittavong V; Wang B, pH-Sensitive metal-free carbon monoxide prodrugs with tunable and predictable release rates. ChemComm. 2017, 53, 9628–9631.

(79). Crook SH; Mann BE; Meijer AJ; Adams H; Sawle P; Scapens D; Motterlini R, [Mn(CO)4{S2CNMe(CH2CO2H)}], a new water-soluble CO-releasing molecule. Dalton Trans. 2011, 40, 4230–4235. [PubMed: 21403944]

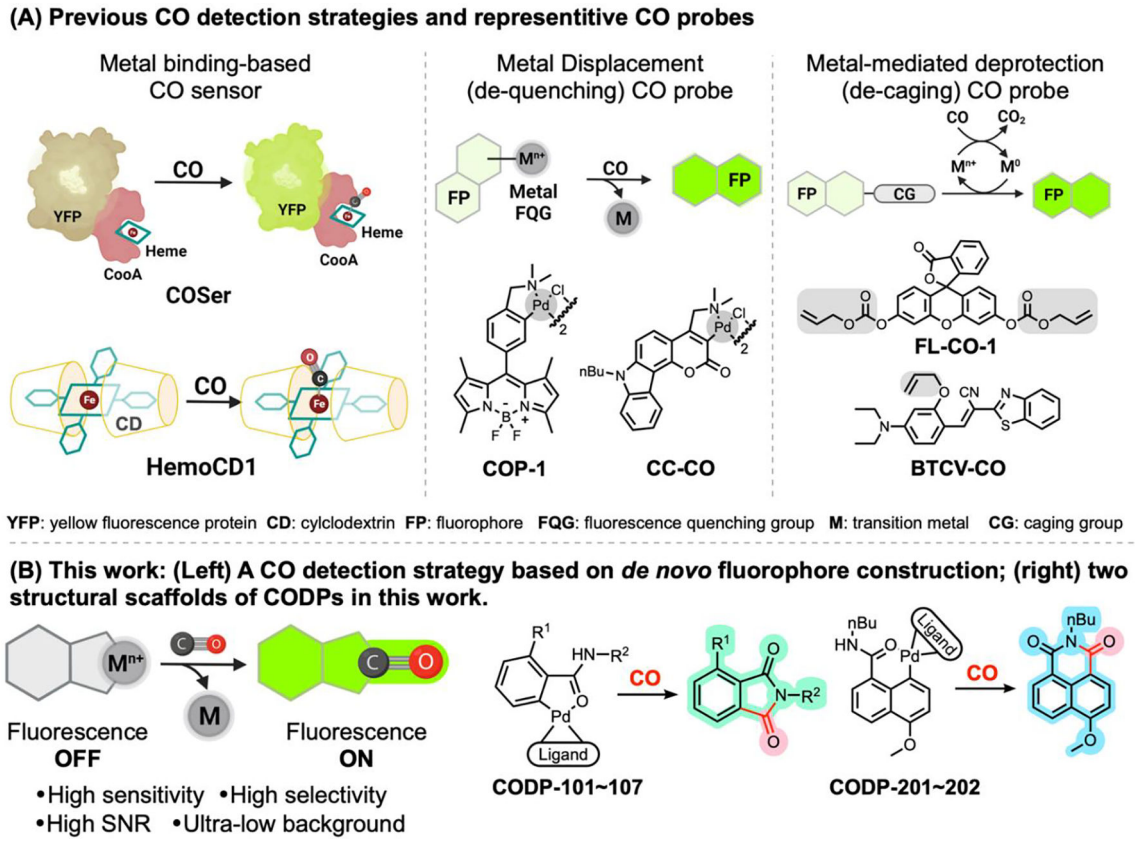

Figure 1.

Comparison of the CO sensing mechanisms and representative probes reported in the literature (**A**) and the probes described in this study (**B**).

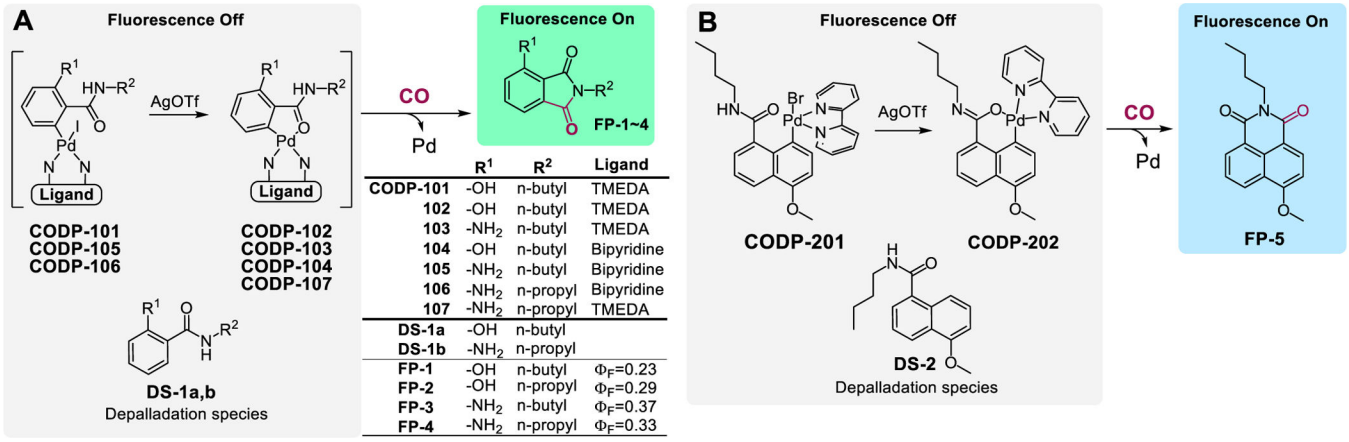

	R^1	R^2	Ligand	
CODP-101	-OH	n-butyl	TMEDA	
102	-OH	n-butyl	TMEDA	
103	$-NH_2$	n-butyl	TMEDA	
104	-OH	n-butyl	Bipyridine	
105	$-NH_2$	n-butyl	Bipyridine	
106	$-NH_2$	n-propyl	Bipyridine	
107	$-NH_2$	n-propyl	TMEDA	
DS-1a	-OH	n-butyl		
DS-1b	$-NH_2$	n-propyl		
FP-1	-OH	n-butyl	Φ_F=0.23	
FP-2	-OH	n-propyl	Φ_F=0.29	
FP-3	$-NH_2$	n-butyl	Φ_F=0.37	
FP-4	$-NH_2$	n-propyl	Φ_F=0.33	

Figure 2.
Design of phthalimide-based CO probes (A) and naphthalimide-based CO probes (B).

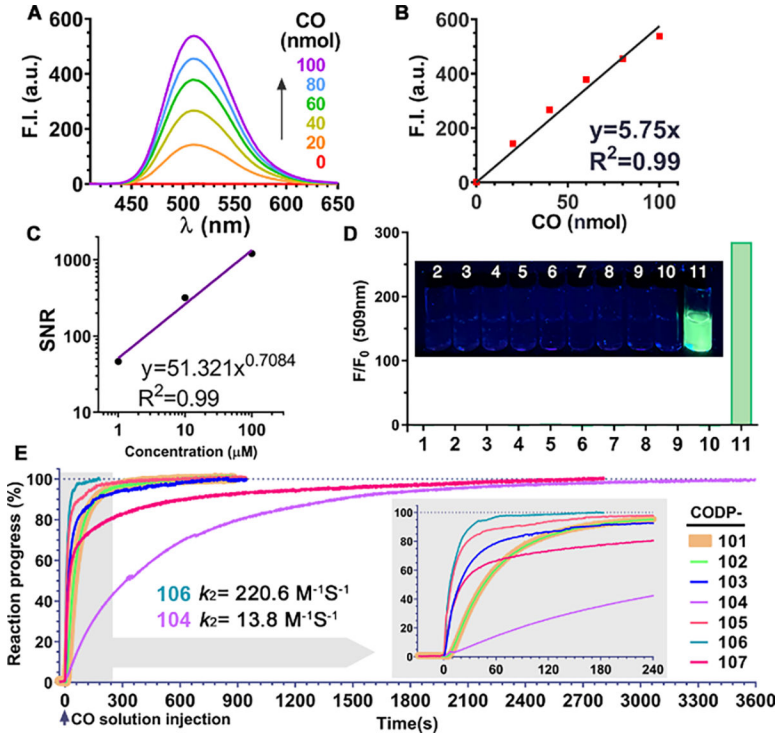

Figure 3.

CO detection profiles of **CODP-10x** series. (A and B) Turn-on fluorescence response of **CODP-102** (500 μM) to CO gas (0–100 nmol) in a headspace vial at 1 h (λ_{Ex} = 394 nm, bandwidth = 5 nm); (C) Regression of SNR *vs.* concentrations of **CODP-102** at 1, 10, and 100 μM in PBS; (D) Selectivity of 20 μM **CODP-102** in pH 7.4 PBS (species: 1: vehicle; 2: Cys; 3: GSH; 4: GSSG; 5: H_2O_2; 6: H_2S; 7: H_2S_2; 8: HClO; 9: NO_2^-; 10: CN^-; 11: 1% CO gas in air at 1 atm (concentration of other species was 100 μM) after 1h incubation (λ_{Ex} = 395 nm, bandwidth = 5 nm); insert: image of incubation solutions; (E) CO detection kinetics of **CODP**s. 800 μL 12.5 μM **CODP**s was mixed with 200 μL 1 mM CO saturated PBS at T_0, and the fluorescence intensity at 509 nm or 499 nm was recorded every second at 25 °C; insert: expanded range of 0–240 s.

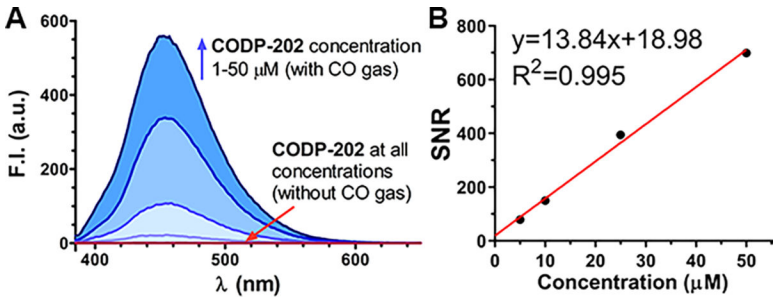

Figure 4.

CO detection SNR of **CODP-202.** (A) **CODP-202** at concentrations of 1, 10, 25, and 50 μM in PBS incubated with or without CO gas for 1 h; (**B**) linear regression of SNR against probe concentration in PBS (bandwidth: ex=3 nm, em=5 nm).

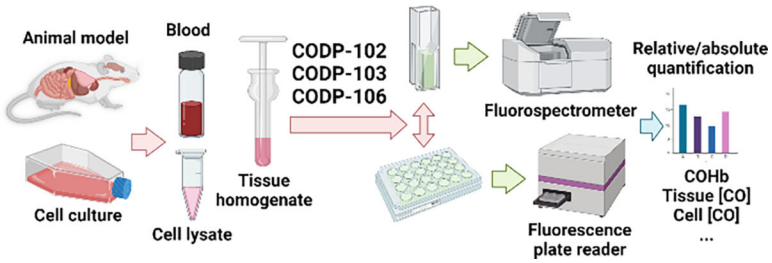

Figure 5.

Application of CODPs to determine CO in biological samples (Figure created with BioRender.com).

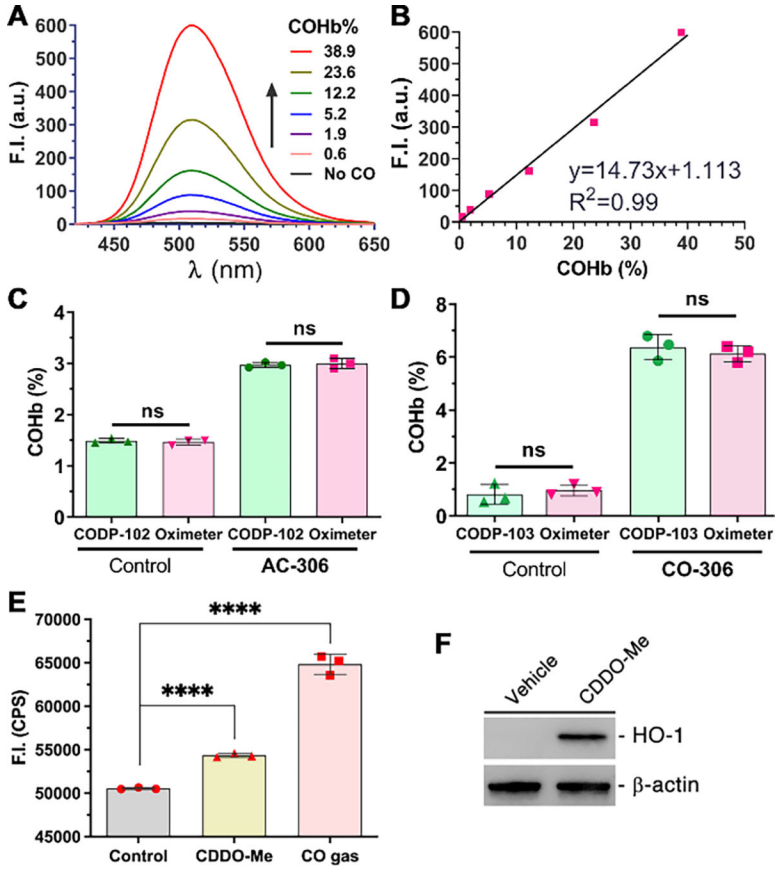

Figure 6.

Spectra (A) and a calibration curve (B) of mouse blood with various COHb levels determined by 10 mM **CODP-102** (λ_{EX} = 395 nm); (C) blood COHb levels of mice dosed with or without AC-306 (50 mg/kg) determined with **CODP-102** and a CO-oximeter; (D) blood COHb levels of mice dosed with or without CO-306 (200 mg/kg) determined with **CODP-103** and a CO-oximeter; (E) relative CO levels of HeLa cells treated with 0.3 μM CDDO-Me (6 h) or 250 ppm CO gas (2 h); (E) Western blot of HO-1 in HeLa cells treated with 0.3 μM CDDO-Me (6 h), β-actin was probed as the loading control. For C-D, results shown as average ± SD (n=3), ****P<0.0001, ns: not significant (P>0.05), t-test.

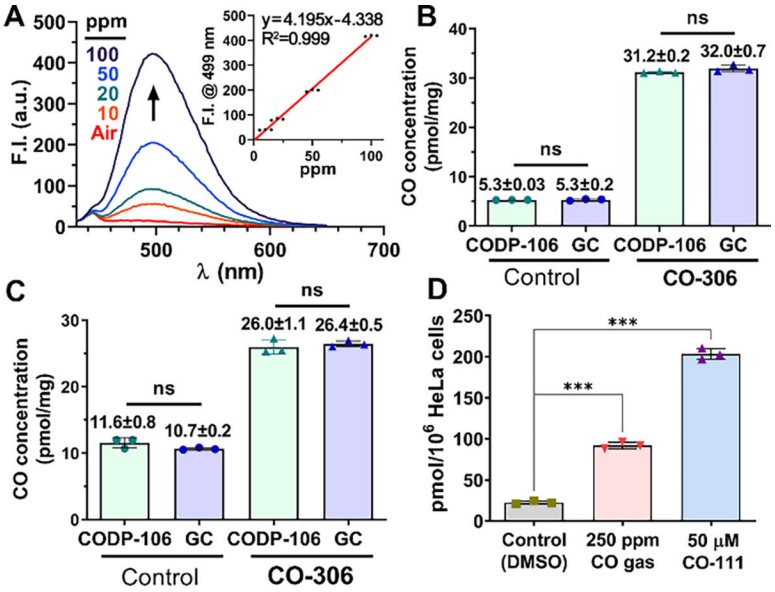

Figure 7.

(A) Fluorescence spectra of 1 mM **CODP-106** in DMA incubated with 10–100 ppm CO calibration gas; insert: calibration curve of CO concentration (ppm) *vs.* fluorescence intensity at 499 nm (λ_{EX} = 385 nm); CO concentrations of the liver (B) and kidney (C) tissues of mice dosed with or without CO-306 (200 mg/kg) determined by **CODP-103** and methanizer-FID-GC; (D) CO concentrations in HeLa cells treated with CO gas or a CO prodrug, **CO-111** (50 μM), for 2 h and tested with **CODP-106**. For B-D, results shown as average ± SD (n = 3), ***P<0.001, ns: not significant (P>0.05), t-test.

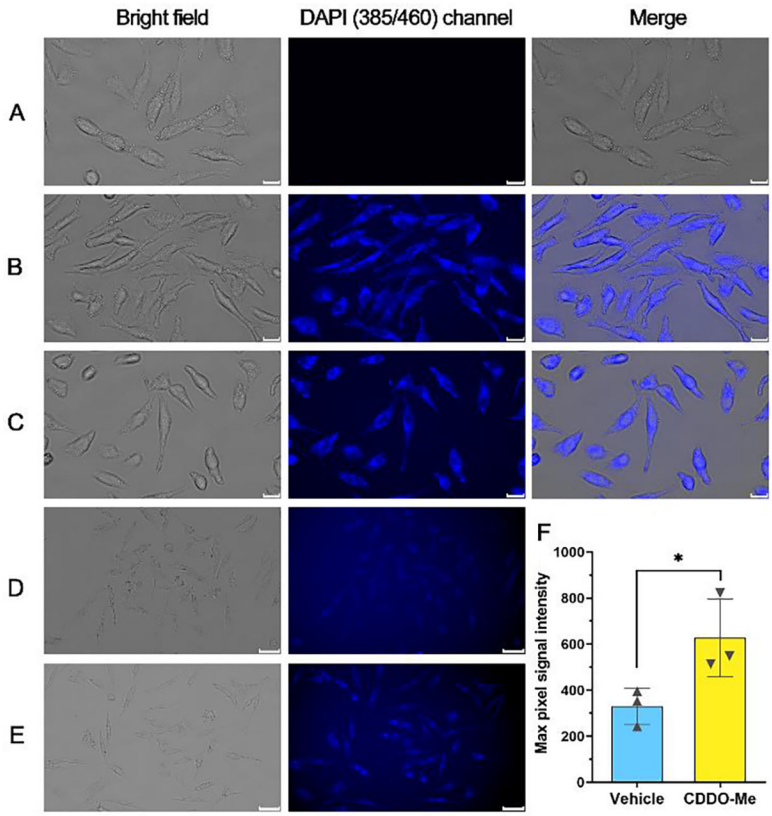

Figure 8.

Fluorescence microscopy image of CO in live cells. HeLa cells were treated with 0.5% DMSO vehicle control (**A**), 250 ppm CO gas (**B**), or 50 μM **CO-201** (**C**) for 1 h followed by addition of 20 μM **CODP-202** and incubation for 1 h (scale bar: 20 μm); HeLa cells were treated with 0.5% DMSO vehicle (**D**), or 0.3 μM CDDO-Me (**E**) for 6 h followed by incubation with 20 μM **CODP-202** for 1h (scale bar: 50 μm). (**F**) Background-normalized maximum signal intensity of the cells in the image (*$*P$* < 0.05, n=3, ROI is shown in Figure S21).

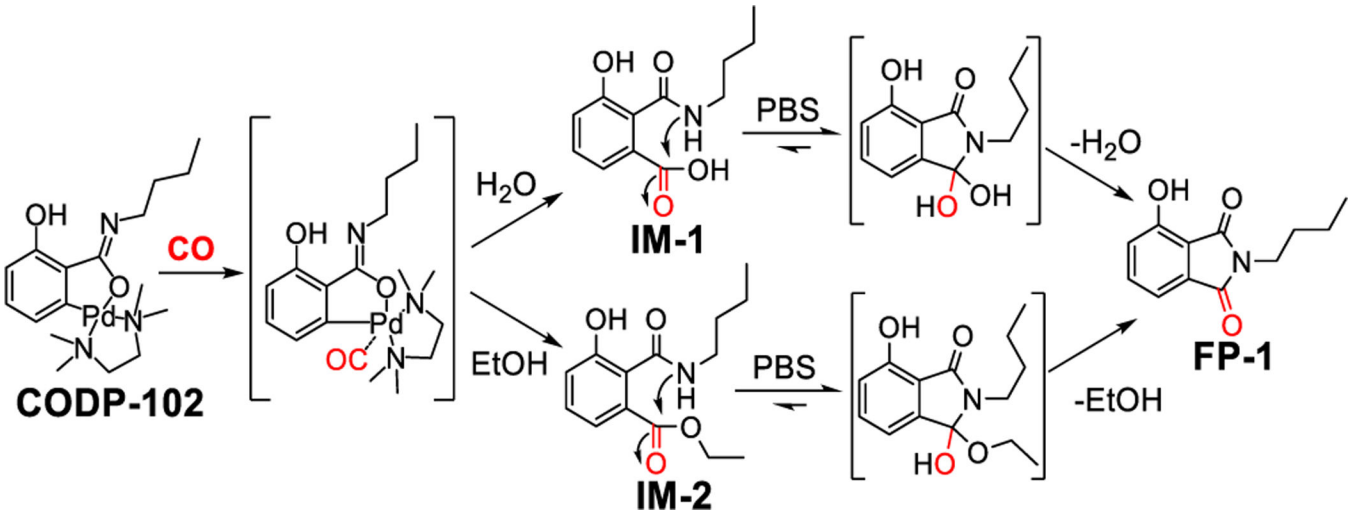

Scheme 1.
Proposed CO detection mechanism of **CODP-102**.